communications biology

A Nature Portfolio journal

Article

https://doi.org/10.1038/s42003-025-07775-9

Preferential allosteric modulation of Otop1 channels by small molecule compounds

Xiangjin Kong[1,2,4], Jie Sun[1,2,4], Hanhan Zhang[3], Yuan Yin[1], Xinyao Liang[1], Yan Chen[1], Guoqing Luo[1], Huixin Xia[1], Youjun Wang[3], Zhonghua Liu[1,2,5] ✉ & Cheng Tang[1,2,5] ✉

The Otopetrin (Otop) proteins, comprising Otop1-3, are proton-gated proton channels with key biological functions. Otop1 acts as a receptor for sour and ammonium salt tastes in mammals, but its gating mechanisms and pharmacology remain poorly understood. Here, we report the functional characterization of three small molecule positive allosteric modulators of Otop1—MFaN, HIMOP, and B2FAMP—that enhance proton gating in a pH-dependent manner, potentiating Otop1 activity under weak acidic but not strong acidic conditions. HIMOP also uniquely enhances Otop1's alkali gating. These modulators preferentially target Otop1, sparing Otop2 and Otop3, and other ion channels. MFaN activates Otop1 while preserving its core biophysical and pharmacological properties by associating with key residues on the channel's S5-6 and S11-12 loops, including a crucial arginine (R554) essential for Zn^{2+} and alkali activation. This study identifies important Otop1 modulators and structural elements underlying its gating, paving the way for further exploration of this ion channel.

Ion channels on the plasma membrane and endomembrane systems in living cells detect external and internal stimuli, converting them into secondary signals such as membrane depolarization/hyperpolarization and ion homeostasis. These signals are then decoded by the cells, regulating downstream activities[1]. The stimuli—including transmembrane voltage, mechanical force, and various ligands, categorize ion channels into three types: voltage-gated, mechanically-gated, and ligand-gated ion channels[1]. Among ligand-gated ion channels, proton-gated ion channels are particularly unique, as: i) protons, primarily produced during cellular respiration, are potentially the smallest biological ligands and ubiquitous in the body[2]; ii) protons can directly gate ion channels[3–5], or act as modulators influencing the gating process in response to other stimuli[6–8], or both[5,9]; iii) proton receptor sites, known as titratable residues including glutamate, asparate, and histidine, are widely distributed on proton-gated ion channels, which greatly complicates the channels' gating regulation. Over a long period of time, only two classical types of proton-gated ion channels had been identified in mammals: the acid-sensing ion channels (ASICs)[4] and the proton-activated chloride channel (PAC)[3]. The H_V1 channel, however, is a proton-conducting channel gated by membrane depolarization[10].

In the complex sensory system that humans have evolved, the tongue detects five basic tastes: sweet, sour, salty, bitter, and umami. These tastes encourage us to seek out nutritious foods and avoid potentially poisonous substances[11]. While the molecular determinants for detecting sweet[12,13], salty[14], bitter[15], and umami[13] were identified long ago, the molecular identity of the receptor for sour taste was only recently uncovered[16,17]. Through a comparative transcriptome analysis of mouse taste receptor cells, the Otopetrin1 (Otop1) protein—previously known for its role in otoconia development in the vestibular system—was identified as a novel proton-selective ion channel mediating the Zn^{2+}-sensitive proton currents in taste receptor cells[18–21]. The other two paralogous members in the Otopetrin family, Otop2 and Otop3, are also proton-conductive channels[21]. Analyzing the gating properties of Otop1-3 confirmed that these three channels, similar to the influenza M2 channel, are proton-gated proton channels[22]. These features differentiate Otop1-3 channels from other ion channels solely gated by or conductive for protons[10]. Importantly, knocking out the Otop1 gene abolished the acid-evoked currents and action potential firing in murine taste receptor cells, and severely diminished gustatory nerve response to acid[16,17]. These findings argued for the Otop1 channel as the primary nociceptor for sour taste.

The Otop1-3 channels are homodimers, with each subunit containing 12 transmembrane segments (S1-12)[23,24]. Segments S1-6 surround to form the N-domain, and segments S7-12 the C-domain, connected by a long

[1]The National and Local Joint Engineering Laboratory of Animal Peptide Drug Development, College of Life Sciences, Hunan Normal University, Changsha, China. [2]Peptide and small molecule drug R&D platform, Furong Laboratory, Hunan Normal University, Changsha, China. [3]Beijing Key Laboratory of Gene Resource and Molecular Development, College of Life Sciences, Beijing Normal University, Beijing, China. [4]These authors contributed equally: Xiangjin Kong, Jie Sun. [5]These authors jointly supervised this work: Cheng Tang, Zhonghua Liu. ✉e-mail: liuzh@hunnu.edu.cn; chengtang@hunnu.edu.cn

intracellular loop. The N-domain of one subunit is adjacent to the C-domain of the other subunit. This distinctive topological arrangement gives the Otop channels a pseudo-tetrameric architecture[23,24]. Seven pore-like structures are revealed in the Otop channels: a central pore surrounded by all four domains, along with putative pores within the N and C domain barrels and the intrasubunit pores located at the interface of the N and C domains[23,24]. The central pore is occluded by cholesterol-like molecules and unlikely conductive of ions[23,24], which is distinct from other canonical ion channels[25,26]. Molecular dynamics simulations suggested that the N- and C-domain pores, as well as the intrasubunit pores are potential proton-conduction pathways[24]. Nontheless, the conserved Gln-Asn/Glu-Tyr constriction triads within the N- and C-domain pores disrupt continuous water wires, leaving their roles in proton conduction uncertain[24]. In the zebrafish Otop1 channel, mutation analysis identified a functional salt bridge in the C-domain pore and conserved charged residues in the intrasubunit pore, both governing proton conduction[24]. Additionally, in the Otop3 channel from Xenopus tropicalis (XtOtop3), mutating the triad motif in the C-domain pore, but not the equivalent residues in the N-domain pore, eliminated channel activity[23]. Beyond this, a substituted cysteine accessibility assay highlighted the role of the D570 residue in the C-domain pore of the human Otop1 channel in proton conduction[27]. Collectively, these findings support the C-domain pore and/or the intrasubunit pore as the bona fide proton conduction pathways, although this assertion still requires further experimental validation.

Multiple lines of evidence revealed the polymodal nature of the gating of Otop channels. Besides protons, alkali and NH_4Cl also gate the Otop1 channel, likely through different mechanisms[28,29]. In particular, the extracellular L5-6 and L11-12 loops of Otop channels were identified as crucial gating apparatus regulating channels' proton gating, as revealed through mutational and chimeric channel analyses[22,27]. This was further supported by using Zn^{2+}, a bifunctional modulator of Otop channels, to probe the key functional elements involved in the channels' proton gating, which demonstrates that Zn^{2+} activates Otop1 and Otop3 channels by correlating with these two loops[30]. Interestingly, these loops are also involved in the alkali gating of the Otop1 channel, with mutations of K221 on L5-6 and R554 on L11-12 fundamentally impairing the channel's alkali gating but not acid gating[28]. In contrast, NH_4Cl gating of the Otop1 channel requires an intracellular arginine residue[29]. Despite these advancements, significant questions remain, particularly about the locations of the proton sensors and pores. It is also unclear whether there exists crosstalk between the proton, alkali, and NH_4Cl gating of the channel or if these stimuli gate the same proton-conducting pathways within the channel.

Pharmacological agents are valuable probes for interrogating the function, gating, and structure-function relationship of ion channels. Zn^{2+} and the compound cibacron blue 3G-A were identified to act on the Otop1 channels, with Zn^{2+} being a bifunctional modulator and the later an antagonist[30,31]. However, these two modulators are of low-potency and poor selectivity to Otop channels, which limited their ultility. Herein, we reported the functional characterization of three potent and preferential positive allosteric modulators (PAMs) of the Otop1 channel, which we designated as MFaN, HIMOP, and B2FAMP, respectively. A in-depth investigation of the action mechanism of MFaN revealed it specifically acted on the channel's acid gating, enhancing Otop1 currents evoked by acid in a pH-dependent manner without affecting the channel's core pharmacological and biophysical properties. A number of residues mutation on the S5-6 loop markedly reduced MFaN's effect, and a common R554A mutation on the S11-12 loop significantly abolished the channel's response to Zn^{2+}, alkali, and MFaN, which argued for a pivotal role of R554 in Otop1's gating. In aggregate, this study identified an important class of modulators acting on the Otop1 channel, characterized key components of its gating mechanism, and laid the groundwork for future research into the channel's function, gating, and pharmacology.

Results

The compounds MFaN, HIMOP, and B2FAMP are positive allosteric modulators of the Otop1 channel

To identify Otop1 modulators which could be used to interrogate the channel's gating, function, and pharmacology, we conducted a screening of a chemical compound library (from Selleck Chemicals LLC, Catalog No. L3600) featuring different core structures and structural diversities through patch-clamp analysis. Specifically, we assessed the impact of compounds (10 μM) on the pH 5.5-evoked currents of mouse Otop1 (mOtop1) channels heterologously expressed in HEK293T cells. When exposed to prolonged acidic pH treatment, the mOtop1 currents exhibited time-dependent decay following peak activation, due to both the disruption of proton gradients across the membrane and to channel desensitization (Fig. 1A). Thus, we sequentially applied pH 5.5 bath solutions, without and with the addition of 10 μM compounds, to evaluate their effects on mOtop1 channels by examining their influence on the current decay (defined as "on-current" analysis). Typically, antagonists would accelerate, while agonists slow or even reverse this process. Of the 4208 compounds tested, we identified three hit compounds with robust potentiation effects on mOtop1 currents — 5-methyl-N-2-naphthyl-2-furamide (CAS: 297138-10-4), (2-hydroxyphenyl)-(3-propan-2-yl-5-isoxazolo[5,4-b]pyridinyl)methanone (CAS: 851797-02-9), and 5-Bromo-N-[4-(2-furoylamino)-3-methylphenyl]-2-furamide (CAS: 505071-89-6), which were designated as MFaN, HIMOP, and B2FAMP, respectively (Fig. 1B). These compounds were synthesized, purified to homogeneity, and structurally validated by NMR assays (Supplementary Figs. 1–3, Supplementary Data 2). At pH 5.5, MFaN, HIMOP, and B2FAMP dose-dependently potentiated mOtop1 currents, with apparent EC_{50}s of 10.3 ± 2.6 μM, 16.8 ± 6.5 μM, and 12.2 ± 3.4 μM, respectively (Fig. 1C). It was observed that these compounds had equivalent potency and efficacy in potentiating mOtop1 currents under condition of the same pH (Fig. 1C). Interestingly, increasing the pH to 6.0 markedly enhanced the efficacy of MFaN, an representative of these three compounds, in potentiating mOtop1 currents, without affecting its apparent potency (Fig. 1C). This suggested a pH-dependent action of MFaN on the mOtop1 channel. We thus explored MFaN's activity across various pH conditions. In response to pH stimuli ranging from 3.5 to 9.5, mOtop1-transfected cells, but not untransfected control cells, developed noticeable currents at both acidic and alkaline pHs, but not at the physiological neutral pH of 7.5 (Fig. 1D). These observations are in line with previous study characterizing Otop1 as a channel activated by both acid and alkali[21,28]. Of particular note, despite significantly potentiating Otop1 currents under acidic conditions, MFaN did not affect mOtop1 activity at either alkaline nor neutral pH, suggesting that it selectively acted on the acid gating of the mOtop1 channel (Fig. 1D, E). Additionally, its efficacy in currents potentiation diminished as the stimuli pH became more acidic, with no detectable effect at pH 3.5 (Fig. 1D, E). These findings strongly argued that MFaN acted on the mOtop1 channel as a positive allosteric modulator (PAM), potentiating the activation effects of protons, by enhancing the channel's proton gating. Similarly, HIMOP and B2FAMP did not potentiate mOtop1 currents at pH 3.5 (Fig. 1F, G), supporting that they acted on the mOtop1 channel as PAMs as well.

We next examined whether MFaN affected the peak currents of mOtop1 channels similarly to the decay phase currents at various pHs. The run-down of mOtop1 peak currents over repeated acid stimuli posed challenges for gauging MFaN's effect in the same recording cell (defined as "on-cell" analysis), particularly in conditions of medium to strong acid stimuli. Thus, we opted to compared the peak current density between two groups of mOtop1-expressed cells, with or without MFaN treatment, across a pH range of 3.5–9.5. As a result, 10 μM MFaN significantly increased the mOtop1 current density at pHs ranging from 4.5 to 6.0, but not at neutral to alkaline pHs or at pHs below 4.0 (Fig. 1H). At pH 6.0, the mOtop1 currents remained relatively stable across repeated stimuli, and we determined the EC_{50} of MFaN against mOtop1 channels as 9.2 ± 0.6 μM through the "on-cell" analysis (Fig. 1I, J). These data align with the results from the

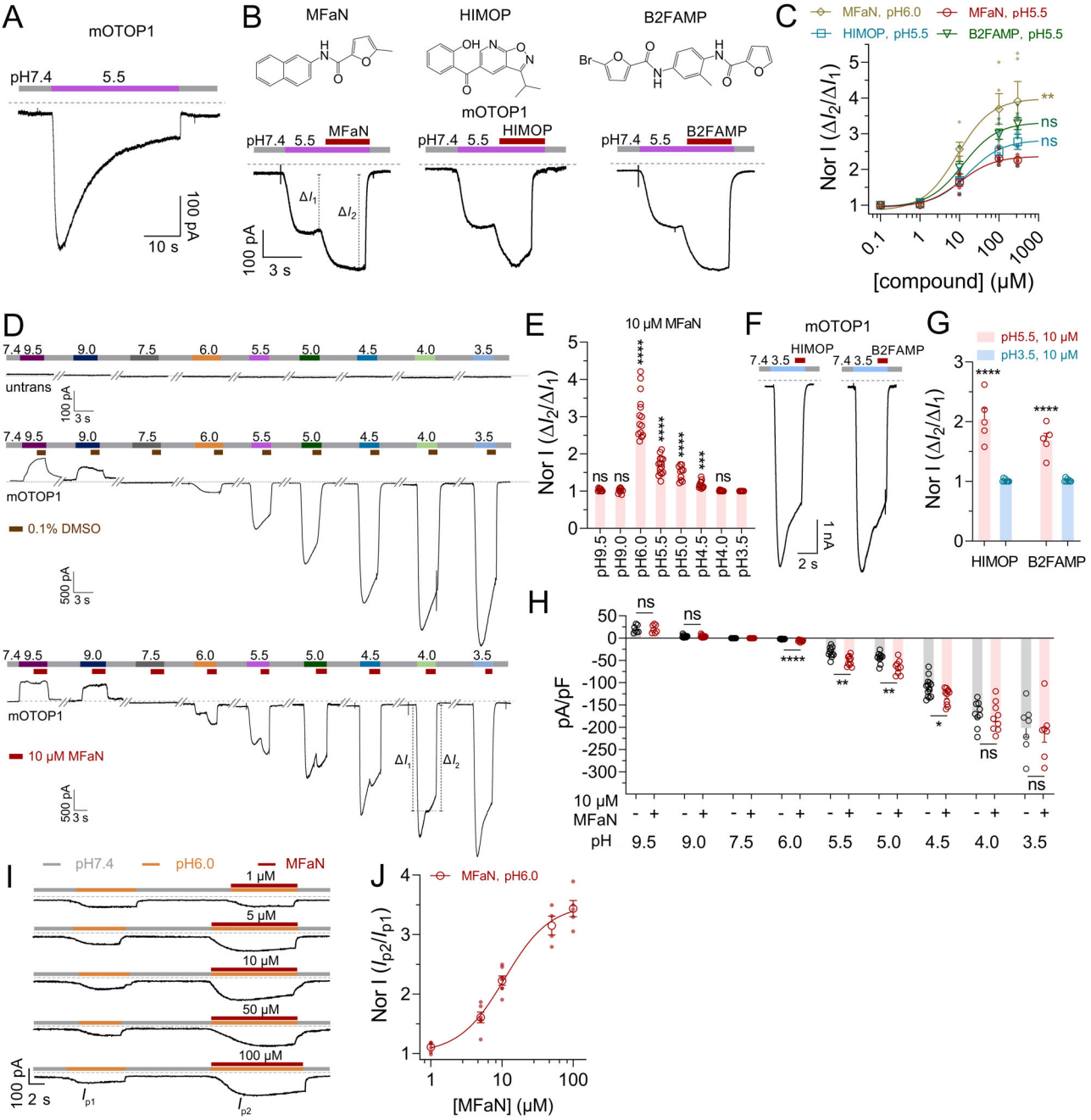

Fig. 1 | Characterization of the compounds MFaN, HIMOP, and B2FAMP as positive allosteric modulators of the Otop1 channel. A Typical pH 5.5-activated currents of mouse Otop1 (mOtop1) channels heterologously expressed in HEK293T cells ($n = 5$). **B** Structures of MFaN, HIMOP, and B2FAMP (upper panels) and typical current traces showing that these compounds (at 10 μM concentration) potently potentiated pH 5.5-activated mOtop1 currents (lower panels). ΔI_1 and ΔI_2 indicate the currents immediately before, and the peak current after compounds treatment, respectively ($n = 5$). **C** Dose-response relationships of compounds potentiating the acid-activated mOtop1 currents, with the EC_{50}s being determined as 10.3 ± 2.6 μM, 16.8 ± 6.5 μM, and 12.2 ± 3.4 μM for MFaN, HIMOP, and B2FAMP at pH 5.5, and 8.9 ± 4.7 μM for MFaN at pH 6.0 ($n = 5$). The maximum $\Delta I_2/\Delta I_1$ ratio of other groups were compared to that of the MFaN/pH 5.5 group. **D** Typical mOtop1 currents activated by alkali/acid stimuli at various pH levels, under conditions without (middle panel; 0.1% DMSO) and with co-administration of MFaN (lower panel; 10 μM), upper panel demonstrates currents recording from untransfected cells ($n = 6$–15). **E** Summary $\Delta I_2/\Delta I_1$ ratio in (**D**) at various pHs, showing MFaN potently potentiated pH 4.5–6.0 acid-activated, but not alkali or pH 4.0 acid-activated mOtop1 currents, when compared to the pH 3.5 group in which the compound did not affect the mOtop1 currents. Each dot represents an independent experimental cell ($n = 6$–15). **F, G** Typical current traces (**F**) and bar statistics (**G**) showing both B2FAMP and HIMOP markedly potentiated pH 5.5 but not pH 3.5-activated mOtop1 currents ($n = 5$–8). **H** Current density (pA/pF) of mOtop1 channels activated by alkali/acid stimuli at different pH levels is shown for conditions without MFaN (black dots) and with co-administration of 10 μM MFaN (red dots). The data demonstrate that MFaN significantly potentiated mOtop1 currents at pH levels between 4.5 and 6.0, but not at other pH levels. Each dot represents an independent experimental cell ($n = 5$–15). **I** Each representative trace illustrates two mOtop1 currents in the same recording cell sequentially evoked by stimuli of pH 6.0 alone (I_{p1}) and pH 6.0 with MFaN (of different concentrations; I_{p2}) ($n = 4$–7). **J** Dose-response relationships of MFaN potentiating pH 6.0-activated mOtop1 currents in (**I**), with the EC_{50} being determined as 9.2 ± 0.6 μM ($n = 4$–7). In these figure panels, currents were recorded at 0 mV for pH values 9.0 and 9.5, and at −80 mV for all other pH values; dotted line indicates the baseline current, and the solution perfusion protocols are as illustrated; Data are presented as MEAN ± SEM. Statistics: ns, not significant; $^*p < 0.05$; $^{**}p < 0.01$; $^{***}p < 0.001$; $^{****}p < 0.0001$; ONE-WAY ANOVA with post-hoc Dunnett analysis in panels (**C**, **E**), and unpaired t-test in panels (**G**, **H**).

aforementioned "on-current" assay. Collectively, we identified three compounds potentiating mOtop1 currents with substantially higher potency than that of the previously reported modulator, Zn^{2+}. Moreover, our comprehensive analysis of MFaN's effects on the mOtop1 channel—considering both decay phase and peak currents, in conditions of different pHs—solidifies the conclusion that MFaN functions as a potent PAM of mOtop1 selectively acting on the channel's acid gating.

MFaN, HIMOP, and B2FAMP enhance cytosal acidification by acting on the Otop1 channel

Otop1 channels mediate H^+ efflux and influx across the cell, affecting the intracellular pH (pH_i). We thus ultilized pH imaging to assess the effects of these three compounds on pH_i by acting on the Otop1 channel. Cells co-expressing ratiometric pH sensor pHmScarlet-mTurquise2 and mOtop1 channels (cpV-mOTOP1) exhibited an upswing in pH_i in response to alkaline stimuli, and a drastically declining pH_i when exposed to acidic extracellular solutions of pH 6.0 or 5.0 (blue traces in Fig. 2A, C, E; and line statistic in Fig. 2B, D, F). In terms of the effects of compounds, we observed that for cells expressing mOtop1 channels, the addition of each of the three compounds at 10 μM significantly increased pH_i changes in response to acidic stimuli (pH 6.0/5.0) (red traces in Fig. 2A, C, E; and line statistic in Fig. 2B, D, F). However, cells expressing mOtop1 channels responded to the alkaline extracellular stimuli with a small but statistically significant increase in pH_i only upon the addition of 10 μM HIMOP (left panels in Fig. 2A, C, E;

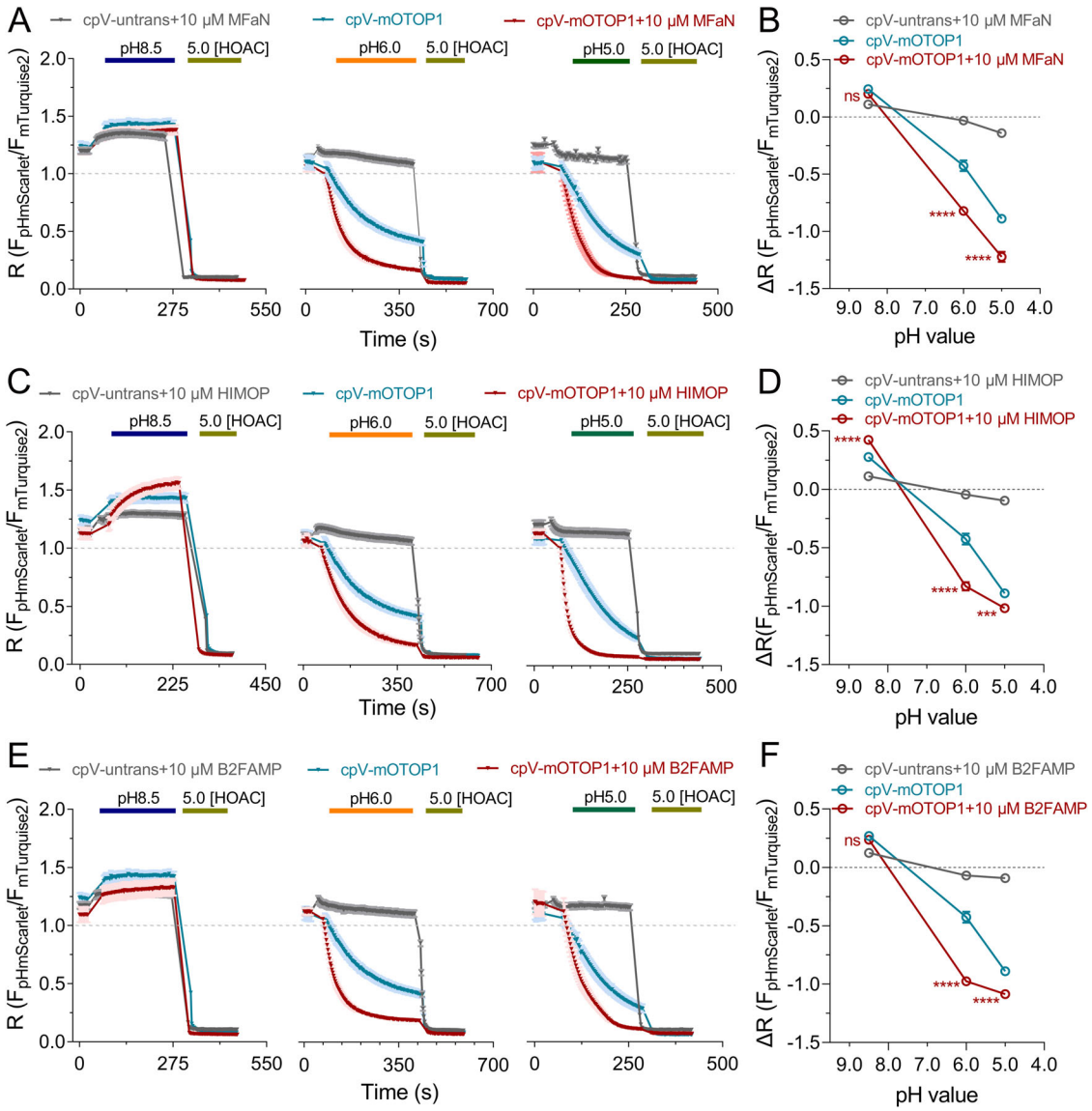

Fig. 2 | Effects of MFaN, HIMOP and B2FAMP (all at 10 μM) on the influx and efflux of protons mediated by mOTOP1 channels in HEK293 cells as measured with intracellular pH imaging. The ratiometric pH indicator pHmScarlet-mTurquise2 (pHmS-mTq2) was expressed in HEK293 cells to record intracellular pH variations as fluorescence ratios (R=FpHmScarlet/FmTurquise2) upon exposure to changing extracellular pH(pH=5.0/6.0/8.5) with mOtop1 channels co-expressed (blue line), or the addition of 10 μM compounds (black line), or both. Cells were bathed in pH 7.4 physiological solution before the pH shift, and compounds were added into the imaging solution at different pH and worked transiently when changing extracellular pH. Acetic acid, which is permeable through cell membranes and acidifies cell cytosol directly, served as a positive control. **A**, **B** 10 μM MFaN increases intracellular pH changes mediated by mOtop1 in response to acidification significantly, but has no effect on alkalinization conditions. **A** Typical traces of changing extracellular pH=5.0/6.0/8.5, respectively (n = 8–25); (**B**) statistics (n = 24–76). **C**, **D** 10 μM HIMOP increases intracellular pH changes mediated by mOtop1 in response to both acidification and alkalinization significantly. **C** Typical traces of changing extracellular pH=5.0/6.0/8.5, respectively (n = 8–26); (**D**) statistics (n = 24–70). **E**, **F** 10 μM B2FAMP increases intracellular pH changes mediated by mOtop1 in response to acidification significantly, but has no effect on alkalinization conditions. **E** Typical traces of changing extracellular pH=5.0/6.0/8.5, respectively (n = 8–17); (**F**) statistics (n = 21–65). Data are presented as MEAN ± SEM. In (**B**, **D**, **F**), statistic was evaluated using unpaired t-test (ns, not significant; ***$p < 0.001$; compared to the cpV-mOtop1 group).

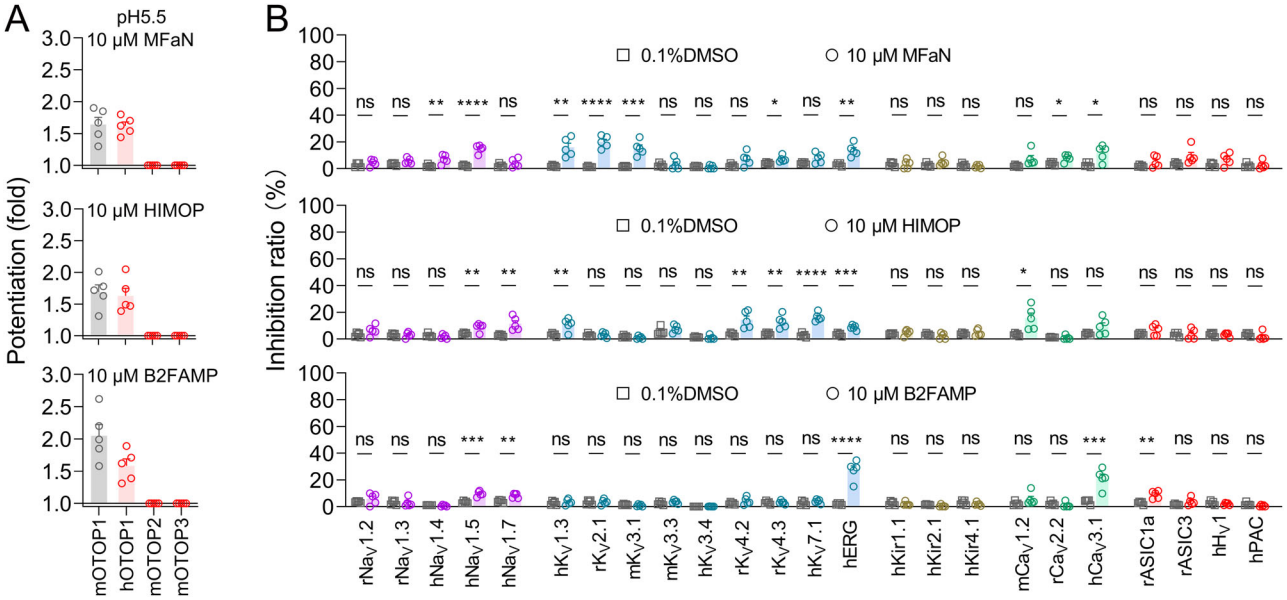

Fig. 3 | MFaN, HIMOP, and B2FAMP preferentially acted on the Otop1 channel. **A** Bar statistics showing that MFaN, HIMOP, and B2FAMP (all at 10 μM) did not affect pH 5.5-evoked currents mediated by mouse Otop2 (mOtop2) and Otop3 (mOtop3) channels, in contrast to their potent potentiation effects on currents mediated by both mouse and human Otop1 (mOtop1 and hOtop1) channels ($n = 5$). **B** Bar statistics summarizing the inhibitory effects of MFaN, HIMOP, and B2FAMP (all at 10 μM) on various off-target ion channels as indicated, showing that these channels were relatively insensitive to all three compounds ($n = 5$). In currents recording for each channel, a bath solution containing 0.1% DMSO was applied prior to compound administration. The current inhibition (inhibition ratio) caused by 0.1% DMSO (open squares) and 10 μM compound (open circles) was compared (ns, not significant; $^{*}p < 0.05$; $^{**}p < 0.01$; $^{***}p < 0.001$; $^{****}p < 0.0001$; unpaired t-test). In (**A**, **B**), each plot represents an independent experimental cell. Data are presented as MEAN ± SEM.

and line statistics in Fig. 2B, D, F). And we hardly observed a response to extracellular pH variation and compounds treatment in cells expressing merely pHmScarlet-mTurquise2 (cpV-untrans) (gray traces in Fig. 2A, C, E; and line statistic in Fig. 2B, D, F). As a positive control, acetic acid (HOAC) of pH 5.0 triggered dramatical pH_i dropdown in both mOtop1 transfected and nontransfected cells, to a extent observed with the addition of acid and the compounds in mOtop1-expressed cells (Fig. 2A, C, E). Collectively, these data indicate that all three compounds are potent modulators for the mOtop1 channel in response to acidic stimuli, while only HIMOP might also play an active role under alkaline conditions.

MFaN, HIMOP, and B2FAMP preferentially act on the Otop1 channel

To further establish MFaN, HIMOP, and B2FAMP as pharmacological tools for dissecting the physiological and pathophysiological functions of Otop1, we sought to assess their selectivity against various off-target channels. First, we observed that these compounds also markedly potentiated currents of Otop1 channels from human origin (hOtop1), similar to their effect on mOtop1, thus ruling out species specificity (Fig. 3A, Supplementary Figs. 4–6). We next examined their activity on the paralogous Otop2 and Otop3 channels. In contrast to Zn^{2+} that potentiated both Otop1 and Otop3 currents, all three compounds at 10 μM concentration were inactive on the Otop2 and Otop3 channels from mouse origin (mOtop2 and mOtop3) (Fig. 3A, Supplementary Figs. 4–6). Furthermore, these compounds exhibited varing degrees of activity against a range of off-target channels, from no effect to weak inhibition at a concentration of 10 μM. Among the 24 tested ion channels, 15 channels ($Na_V1.2$, $Na_V1.3$, $Na_V1.7$, $K_V3.3$, $K_V3.4$, $K_V4.2$, $K_V7.1$, Kir1.1, Kir2.1, Kir4.1, $Ca_V1.2$, ASIC1a, ASIC3, H_V1, and PAC), 16 channels ($Na_V1.2$, $Na_V1.3$, $Na_V1.4$, $K_V2.1$, $K_V3.1$, $K_V3.3$, $K_V3.4$, Kir1.1, Kir2.1, Kir4.1, $Ca_V2.2$, $Ca_V3.1$, ASIC1a, ASIC3, H_V1, and PAC), and 19 channels ($Na_V1.2$, $Na_V1.3$, $Na_V1.4$, $K_V1.3$, $K_V2.1$, $K_V3.1$, $K_V3.3$, $K_V3.4$, $K_V4.2$, $K_V4.3$, $K_V7.1$, Kir1.1, Kir2.1, Kir4.1, $Ca_V1.2$, $Ca_V2.2$, ASIC3, H_V1, and PAC) were completely resistant to MFaN, HIMOP, and B2FAMP treatment, respectively (Fig. 3B, Supplementary Figs. 4–6). For the ion channels that exhibited weak inhibition by the compounds, the inhibition ratios were ranked as follows: for MFaN, $K_V2.1$ (20.0%) > $K_V1.3$ (15.9%) ≈ $K_V3.1$ (15.2%) ≈ $Na_V1.5$ (14.8%) ≈ hERG (13.7%) > $Ca_V3.1$ (11.7%) > $Ca_V2.2$ (7.9%) ≈ $K_V4.3$ (7.0%) = $Na_V1.4$ (7.0%); for HIMOP, $K_V7.1$ (16.4%) ≈ $Ca_V1.2$ (15.6%) ≈ $K_V4.2$ (14.3%) > $K_V4.3$ (12.9%) ≈ $Na_V1.7$ (11.3%) ≈ $K_V1.3$ (10.8%) > $Na_V1.5$ (8.9%) ≈ hERG (8.5%); and for B2FAMP, hERG (27.2%) > $Ca_V3.1$ (21.1%) > $Na_V1.5$ (9.6%) ≈ ASIC1a (9.0%) ≈ $Na_V1.7$ (8.3%) (Fig. 3B, Supplementary Figs. 4–6). Notably, the $Ca_V1.2$[32], $Na_V1.2$ and/or $Na_V1.3$[33,34], and Kir2.1 channels are known to be expressed in type III taste receptor cells, in which they cooperated to trigger action potential (AP) firing after a protons influx mediated by the Otop1 channel. The specific action of MFaN, HIMOP, and B2FAMP on Otop1 but not these channels promised to enhance the activity of type III receptor cells in response to acid stimulus. In aggregate, these data suggested MFaN, HIMOP, and B2FAMP preferentially acted on the Otop1 channel, with promising use in uncovering the undetermined function of Otop1 in the future.

MFaN does not alter Zn^{2+} inhibition, activation rate, or ion selectivity of the Otop1 channel

Considering that MFaN, HIMOP, and B2FAMP similarly acted on the Otop1 channel as PAMs, we opted to examine whether MFaN, as a representative compound, affected the core pharmacological and biophysical properties of the Otop1 channel. At pH 5.5, 10 μM MFaN significantly increased mOtop1 current density in HEK cells, and it was found that 1 mM Zn^{2+} inhibited the mOtop1 currents activated by acid alone or acid and 10 μM MFaN to the same extent (Fig. 4A). Moreover, the dose-response relationships of Zn^{2+} inhibiting the mOtop1 currents under these two conditions were superimposed (Fig. 4B), suggesting MFaN acted on the mOtop1 channel without affecting its inhibition by Zn^{2+}. Next, we explored the influence of MFaN on the biophysical properties of the Otop1 channel, specifically its activation rate and ion selectivity. Protons directly gate the Otop1 channel, thus the binding of protons to the Otop1 channel is a rate-limiting step in determing its activation. We compared the activation time constant ($\tau_{activation}$) of mOtop1 channel activated by protons alone versus protons with MFaN. Our results showed that MFaN treatment, whether

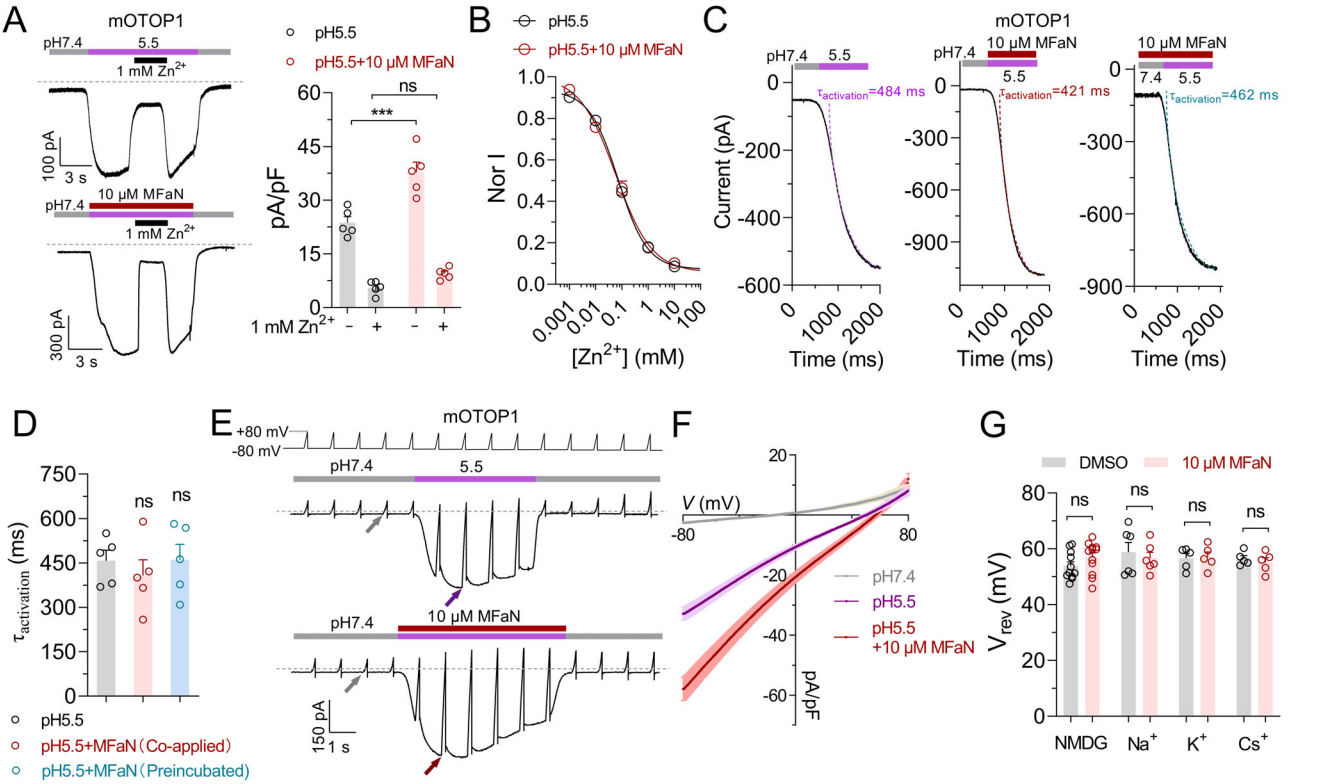

Fig. 4 | MFaN enhanced the proton gating of the mOtop1 channel without affecting its inhibition by Zn^{2+}, activation rate, and ion selectivity. A Typical traces (left panels) and statistics (right panel) illustrating similar inhibitions by 1 mM Zn^{2+} on mOtop1 currents activated by pH 5.5 alone (left upper panel) and pH 5.5 with 10 μM MFaN (left lower panel), currents were elicited using the provided solution perfusion protocols and recorded at -80 mV ($n = 5$). **B** Dose-response relationships of Zn^{2+} inhibiting mOtop1 currents activated by pH 5.5 alone or pH 5.5 with 10 μM MFaN, with the IC_{50}s determined as 72 ± 9 μM and 58 ± 13 μM, respectively ($n = 5$– 6). **C** Representative fitting analysis of the activation phase of mOtop1 currents activated by pH 5.5 alone (left panel) or pH 5.5 with 10 μM MFaN (either concurrently administrated or preincubated; middle and right panels) ($n = 5$). **D** Summary activation time constants from (**C**), showing that MFaN did not affect the activation rate of mOtop1 channels ($n = 5$). **E** mOtop1 currents were elicited by pH 5.5 alone (upper panel) or by pH 5.5 with 10 μM MFaN (lower panel) and recorded at the holding potential of -80 mV with 1 Hz voltage ramp from −80 mV to +80 mV (1 mV/ms). Purple and red arrows indicate the maximum voltage ramp-activated currents which were used to determine the channel's reversal potential (V_{rev}), and gray arrows indicate the background voltage ramp-activated currents at pH 7.4. Note that the bath solution contains $NMDG^+$ as the main cation. **F** Arrow-labeled currents in (**E**) were normalized to the cell capacitance, showing the averaged current density (MEAN ± SEM)-voltage relationships of mOtop1 channels, with MFaN robustly potentiating mOtop1 currents without affecting the channel's V_{rev} ($n = 9$–13). **G** Summary V_{rev} comparison of mOtop1 channels activated by pH 5.5 alone or pH 5.5 with 10 μM MFaN in bath solutions containing the $NMDG^+$, Na^+, K^+, or Cs^+ (all at a concentration of 160 mM) as the main cation ($n = 5$–13). Data are presented as MEAN ± SEM. In (**A**, **D**, **G**), significant differences between groups were evaluated using unpaired t-test (***$p < 0.001$; ns, not significant).

administrated before or concurrently with pH 5.5 acid stimulus, had no effect on the activation rate of mOtop1 channels, as demonstrated by unaltered $\tau_{activation}$ values (Fig. 4C, D). These findings also suggested MFaN associated with the Otop1 channel quickly, akin to protons. Lastly, we investigated MFaN's impact on the ion selectivity of Otop1 channels by examining its influence on the channels' reversal potential (V_{rev}). It was worth noting that we determined the V_{rev} at the time point of maximum current activation during acid perfusion, utilizing a sequence of voltage ramp from −80 mV to +80 mV at a frequency of 1 Hz, which assures to minimize the influence of incomplete solution exchange on V_{rev} calculation (Fig. 4E). As a result, 10 μM MFaN treatment did not change the V_{rev} of the mOtop1 channel compared to the respective control of pH 5.5 alone, both in bath solution containing $NMDG^+$ and those with $NMDG^+$ replaced with other cation species of Na^+, K^+, or Cs^+ (Fig. 4F, G). In summary, these data provided strong evidence that MFaN likely potentiated the activation of Otop1 channels without affecting its core intrinsic pharmacological and biophysical properties.

The molecular mechanisms of MFaN acting on the Otop1 channel

MFaN acted on the proton gating machinery of the Otop1 channel, serving as a valuable molecular tool to probe the proton gating apparatus. Previous studies highlighted the significance of the S5-6 and S11-12 loops on Otop1 in mediating acid gating[22,27,30]. We thus conducted an alanine scan mutation targeting these two loops to identify key residues involved in the action of MFaN. Regarding the S5-6 loop, 23 out of 45 mutants were functionally expressed in HEK cells, as illustrated by significant pH 5.5-evoked currents. Various mutations profoundly affected MFaN's effect, with mutants such as E226A, T233A, I239A, T240A, I241A, and D244A showing markedly reduced, while E229A, L243A, D245A, and H246A significantly enhanced response to MFaN (10 μM) compared to the wild-type mOtop1 channel at pH 5.5 (Fig. 5A). It was especially notable that mutating the R554 residue on the S11-12 loop rendered the channel entirely unresponsive to MFaN, without affecting Zn^{2+} inhibition, underscoring its pivotal role in mediating MFaN's effects (Fig. 5A, B). Interestingly, the R554A mutation similarly impaired Zn^{2+} potentiation, as well as alkali activation of Otop1[28,30]. This implies a cross talk between their actions on the Otop1 channel. MFaN acted on the Otop1 channel pH-dependently, with its efficacy being reduced as pHs approaching the channel's saturating activation pH (Fig. 1E). To confirm that the apparent reduction in MFaN efficacy in these mutant channels was due to the mutation itself rather than a pH-dependent artifact, we further assessed the effect of MFaN on them at a less acidic pH of 6.0. Consequently, mutating E226, T233, I239, and I241, but not T240 and D244, remarkably reduced MFaN's efficacy of currents potentiation at both pHs, arguing for the critical roles of the former four residues (Fig. 5C, D).

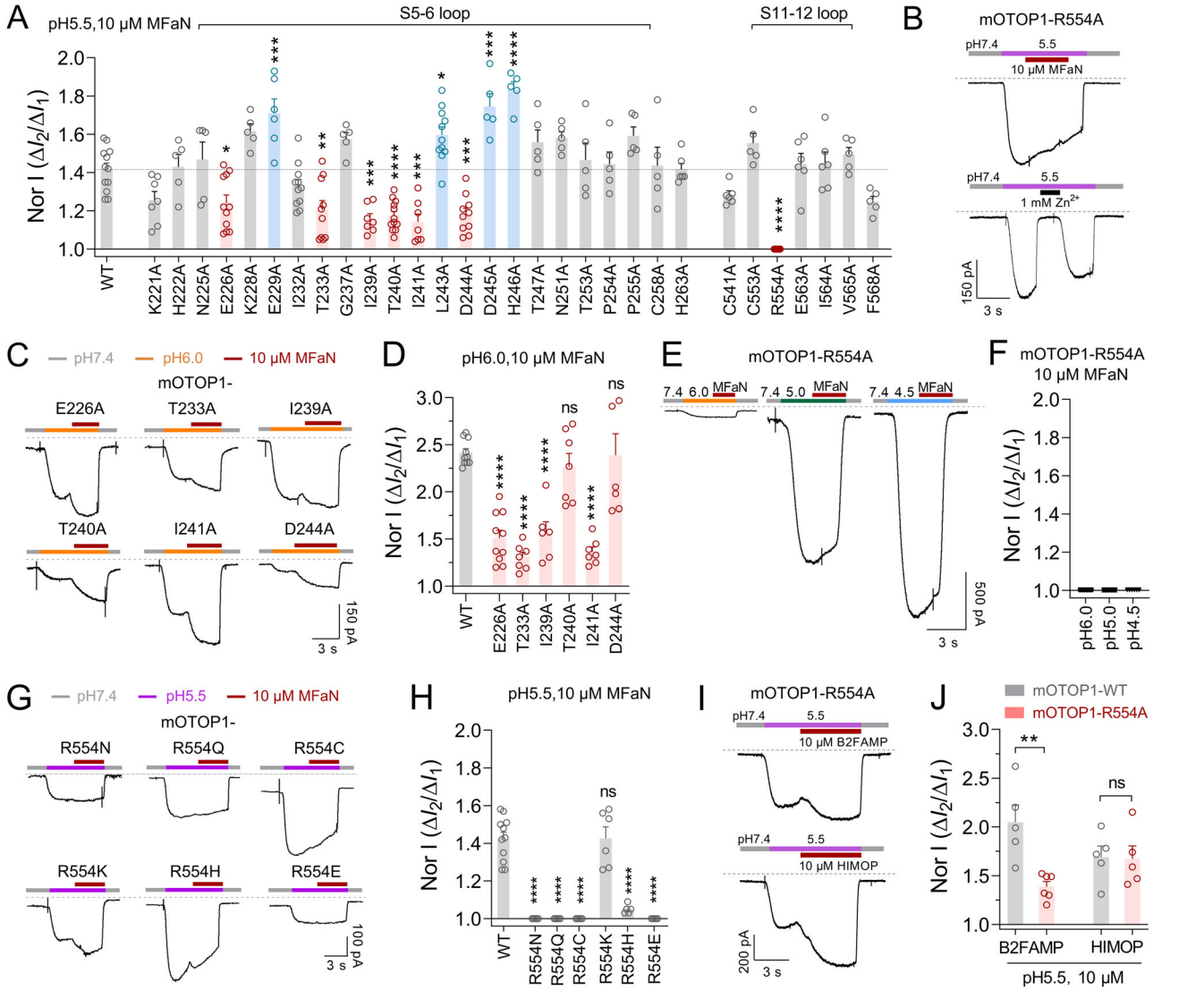

Fig. 5 | Key molecular determinants affecting MFaN's action on the mOtop1 channel. A Summary bar graph illustrating the effects of MFaN (10 μM) on pH 5.5-evoked currents of mOtop1 mutants constructed by alanine-scan mutagenesis of the channel's S5-6 and S11-12 loops. Mutations at E226, T233, I239, T240, I241, or D244 on the S5-6 loop remarkably reduced MFaN's effect, while the R554 mutation on the S11-12 loop eliminated it. In contrast, mutations at E229, L243, D245, or H246 on the S5-6 loop significantly enhanced MFaN's effect ($n = 5–12$). **B** Typical traces showing that the mOtop1/R554A mutant channel was unaffected by MFaN (upper panel) but significantly inhibited by 1 mM Zn^{2+} (lower panel). **C**, **D** Typical current traces (**C**) and statistics (**D**) showing that E226A, T233A, I239A, and I241A, but not T240A and D244A mutations significantly attenuated MFaN's effect on pH 6.0-evoked currents compared to the wild-type (WT) mOtop1 ($n = 6–10$). **E**, **F** Typical current traces (**E**) and a statistical bar graph (**F**) showing that the mOtop1/R554A mutant channel is completely insensitive to MFaN across various pH levels ($n = 6$). **G**, **H** Typical current traces (**G**) and statistics (**H**) showing that R554N, R554Q, R554C, and R554E mutations eliminated MFaN's potentiation effect; R554H reduced it, and R554K did not affect it compared to WT mOtop1 ($n = 5–6$). **I**, **J** Representative current traces (**I**) and statistics (**J**) showing that B2FAMP, but not HIMOP, had a reduced effect on mOtop1/R554A compared to WT mOtop1 ($n = 5$, 6). Data are presented as MEAN ± SEM. Significant differences were assessed using ONE-WAY ANOVA with post-hoc Dunnett analysis (**A**, **D**, **H**), or unpaired t-test (**J**); ns, not significant; $*p < 0.05$; $**p < 0.01$; $***p < 0.001$; $****p < 0.0001$.

The R554A mutant channel remained completely unresponsive to MFaN across pHs of 4.5, 5.0, and 6.0 (Fig. 5E, F). A multiple-attribute mutation analysis revealed that the R554N, R554Q, R554C, and R554E mutants phenocopied the R554A mutant channel, while the R554K mutant behaved similarly to the wild-type mOtop1 channel under MFaN influence (Fig. 5G, H). The R554H mutant channel, however, remained responsive but displayed a significantly reduced potentiation effect by MFaN (Fig. 5G, H). We extended to test the the activity of B2FAMP and HIMOP on the R554A mutant channel, which demonstrated that the mutation remarkably reduced the activity of B2FMAP but not HIMOP (Fig. 5I, J). The mutation analysis could not distinguish between the binding effect and the gating effect[35], leaving uncertainty regarding the precise roles of these identified residues in directly binding with MFaN or facilitating channel opening without being directly involved in MFaN binding. Nevertheless, these data provided compelling pharmacological evidences pinpointed the S5-6 and S11-12 loops, particularly the R554 residue in the later, as crucial components constituting the proton gating apparatus of the Otop1 channel.

Discussion

This study reports the discovery and functional characterization of three small molecule compounds—MFaN, HIMOP, and B2FAMP—that preferentially and potently act as positive allosteric modulators of the Otop1 channel by regulating its acid gating. Through an in-depth investigation of MFaN's action on the Otop1 channel, we identified key common gating apparatus underlying the channel's gating regulation by MFaN, Zn^{2+}, and alkali. Overall, our findings offer new insights into the pharmacology and

gating mechanisms of the Otop1 channel, while also providing an important class of pharmacological tools for future structural and functional studies of this channel.

Pharmacological modulators specifically targeting the Otop1 channel are scarce. Among those identified, Zn^{2+} serves as a bifunctional modulator[21,30], and the compound Cibacron Blue 3G-A acts as a moderate antagonist[31]. However, both lack specificity for the Otop1 channel. Zn^{2+} affects multiple ion channels[36,37], while Cibacron Blue 3G-A is a non-specific ligand commonly used in protein affinity-purification, with strong binding affinities for proteins and enzymes. This lack of specificity significantly limits their utility in studying Otop1 channels. Recently, carvacrol was identified as a novel agonist of the mOtop1 channel, activating Otop1 currents under both neutral and acidic conditions, with a sub-millimolar EC_{50} (approximately 700 μM)[38]. The compounds MFaN, HIMOP, and B2FAMP, identified in the present study, preferentially and potently (EC_{50}s of around 10 μM) enhance acid-evoked Otop1 currents in a pH-dependent manner, without directly activating the channel. These three compounds represent a novel class of modulators, functioning as positive allosteric modulators (PAMs) that act on the channel's proton gating. Mechanistically, they may facilitate proton binding to the channel, promote the transition of protonated channels from closed to open states, or even increase the channel's single-channel conductance. This increase in conductance could occur if the channel has multiple opening states with varying conductances, as seen in other ion channels such as ionotropic glutamate receptors[39]. Regardless of the exact mechanism, these compounds only potentiate Otop1 currents under mildly acidic conditions, where channel activation is not fully saturated—the opening probability (P_o) does not reach 1, and/or the single-channel conductance does not reach its maximum. In pH imaging assays, HIMOP—but not the other two compounds—was found to slightly but significantly enhance the pH_i change in Otop1-expressing cells in response to an alkaline pH 8.5 stimulus. This indicates that HIMOP activates the channel's alkali gating. To investigate further, we evaluated HIMOP's effects on alkali-evoked Otop1 currents. The pH_i decrease occurred gradually following the co-administration of HIMOP and alkaline stimulation (Fig. 2C), suggesting a relatively slow action of HIMOP on Otop1 channels under these conditions. To address this, we preincubated HIMOP with Otop1 channels at pH 7.4 for 2 min during patch-clamp analysis to allow sufficient binding. As expected, preincubated HIMOP significantly enhanced Otop1 currents in response to pH 8.5 stimulation, confirming HIMOP's role in modulating the channel's alkali gating (Supplementary Fig. 7).

To rule out the possibility that the observed variation in activity of MFaN, HIMOP, and B2FAMP across different pHs was due to their differing ionization states, we calculated the theoretical pK_a values of potentially ionizable groups in these compounds using MolGpka (https://xundrug.cn/molgpka)[40], and determined their ionized ratios across the pH range of 3.5–9.5 (Supplementary Table 1 and Supplementary Fig. 8). The results showed that both MFaN and B2FAMP remained uncharged across the entire pH range (Supplementary Fig. 8). In contrast, HIMOP displayed significant deprotonation at its phenolic hydroxyl group as pH increased (Supplementary Fig. 8). Nonetheless, the proportion of deprotonated HIMOP species only slightly decreased from approximately 3.8% at pH 5.5 to 0% at pH 3.5 (Supplementary Fig. 8). This minor change in ionization is unlikely to account for the drastic shift in its activity on acid-evoked Otop1 currents at these two pHs (Fig. 1G). Moreover, it appears that the deprotonated HIMOP species may contribute to the potentiation of Otop1 activity at alkaline pHs (Supplementary Table 1 and Supplementary Fig. 8).

Our data showed that mutating the R554 residue on the L11-12 loop of the Otop1 channel completely abolished the channel's response to MFaN, highlighting the dominant role of this residue in mediating the potentiation effects of the compound. Given that R554 is also pivotal in the channel's gating regulation by Zn^{2+} and alkali[28,30], these findings argued that R554 is a key element of the channel's gating apparatus. Interestingly, mutating R554 only partially reduced the effect of B2FAMP and did not affect HIMOP's action on the Otop1 channel, indicating significant differences in the action mechanisms of the three modulators. Beyond R554, multiple residues on the L5-6 loop of the Otop1 channel are also deeply involved in the action of MFaN, likely reflecting a functional coupling between the L5-6 and L11-12 loops. Indeed, a previous study has proposed that these two loops are in close proximity within the C-pore of the Otop1 channel[27]. Our data support the idea that MFaN binds to the C-pore of the Otop1 channel, associating with the L5-6 and L11-12 loops. However, it's worth noting that the binding pocket of MFaN on the Otop1 channel remains to be precisely located in future studies, as mutation analysis could not distinguish between binding and gating effects[35].

The structural-function relationship study of Otop channels is still in its infancy. Key aspects, such as the location of the proton-conductive pores and the mechanisms of proton gating, remain elusive. Adding to the complexity, the Otop1 channel is polymodally gated by protons, NH_4Cl, and alkali[22,27–30], but it is still unclear whether and how these gating pathways interact. Regarding the channel's proton gating, it is crucial to identify the specific proton sensors whose protonation initiates channel activation. In our previous study, we unbiasedly identified the proton sensors of the proton-activated chloride channel by performing alanine-scanning mutagenesis of all protonatable residues and conducting electrophysiological function assays[41]. However, the situation is far more complicated for Otop channels, as they are both gated by and conductive for protons—a mutation in a protonatable residue might disrupt the proton sensor, the proton conductive pathway, or both. Recently, a structural investigation of the *Caenorhabditis elegans* OTOP8 (CeOtop8) and mouse Otop2 (mOtop2) channels insightfully proposed that these channels utilize a rate-limiting, transporter-like proton conduction mechanism, in which proton transfer is mediated by a glutamate-histidine bridge[42]. It remains unclear whether this mechanism also applies to the Otop1 channel, as it does not exhibit a rate-limiting feature in proton transfer. In contrast, Otop1 currents do not saturate across the tested pH range[22].

MFaN, HIMOP, and B2FAMP are PAMs targeting the channel's acid gating, making them invaluable pharmacological tools for uncovering the channel's structure-function relationships. Presumably, they may act as "molecular glues", stabilizing the channel's activated state. Future efforts could focus on resolving the complex structure of Otop1 in conjunction with these PAMs, potentially capturing the Otop1 channel in its open state and shedding light on the proton-conductive pathway and gating mechanisms. Additionally, the compound HIMOP, which appears to regulate both proton and alkali gating of the Otop1 channel, could serve as a valuable tool to explore potential interactions between these gating mechanisms. While the function of the Otop1 channel is well-characterized in taste receptor cells mediating sour and NH_4Cl sensation[16,17,29], its roles in other physiological and pathological contexts remain unknown. Therefore, the three preferential modulators identified in this study could serve as invaluable pharmacological tools for future functional investigation of Otop1 channels as well.

Materials and methods

Compounds

The Otop1-reactive compounds MFaN (5-methyl-N-2-naphthyl-2-furamid), HIMOP((2-hydroxyphenyl)-(3-propan-2-yl-5-isoxazolo[5,4-b]pyridinyl)methanone), and B2FAMP(5-bromo-N-[4-(2-furoylamino)-3-methylphenyl]-2-furamide) were identified by the gold-standard manual patch-clamp screening against a commercially-available compounds library from Selleck (Selleck Chemicals LLC, Catalog No. L3600). Specifically, mouse Otop1 (mOtop1) channels were transiently expressed in HEK293T cells, and compounds were diluted to a final concentration of 10 μM in a pH 5.5 bath solution containing 0.1% DMSO. The effect of each compound on Otop1 currents, evoked by the pH 5.5 stimulus, was assessed. Each compound was tested in three independent replicates. These hit compounds were synthesized by Beyotime Biotechnology (Beyotime Biotechnology, Shanghai, China), and their purity was confirmed to be >98% through HPLC analysis and structures validated by NMR assay (Supplementary Figs. 1–3, Supplementary Data 2). HPLC purification was carried

out using an analytical C18 column (4.6 × 150 mm, 5 μm, Waters Corporation) with a 6.5 min linear gradient of acetonitrile, increasing from 50% to 95% at a flow rate of 1.5 mL/min. For NMR analysis, the sample was dissolved in $CDCl_3$. ^{13}C-NMR spectra were recorded at 100.61 MHz, and ^{1}H-NMR spectra at 400.13 MHz. Compounds were dissolved in DMSO to make stock solutions of 100 mM and stored at −80 °C. Working solutions were prepared by diluting the stock solution with specific bath solutions by ≥ 1000 folds, minimizing the influence of DMSO in the designated assays.

Plasmids and site-directed mutation

cDNAs encoding Otop1 (*Mus musculus and Homo sapiens*, accession numbers: NM_172709 and NM_177998), Otop2 (*Mus musculus*, accession number: NM_172801), and Otop3 (*Mus musculus*, accession number: NM_001347647.1) were subcloned in the pcDNA3.1-3×Flag-C (Otop1) or pcDNA3.1 (Otop2 and Otop3) plasmids. cDNAs of $Na_V1.2$ (*Rattus norvegicus*, accession number: NM_012647.3), $Na_V1.3$ (*Rattus norvegicus*, accession number: NM_013119.2), $Na_V1.4$ (*Homo sapiens*, accession number: NM_000334.4), $Na_V1.5$ (*Homo sapiens*, accession number: NM_198056.3), $Na_V1.7$ (*Homo sapiens*, accession number: NM_002976.4), $K_V1.3$ (*Homo sapiens*, accession number: NM_002232.5), $K_V2.1$ (*Mus musculus*, accession number: NM_008420.4), $K_V3.1$ (*Mus musculus*, accession number: NM_001112739.2), $K_V3.3$ (*Mus musculus*, accession number: NM_008422.3), $K_V3.4$ (*Homo sapiens*, accession number: NM_004978.6), $K_V4.2$ (*Rattus norvegicus*, accession number: NM_031730.2), $K_V4.3$ (*Rattus norvegicus*, accession number: NM_031739), $K_V7.1$ (*Homo sapiens*, accession number: NM_181798), hERG (*Homo sapiens*, accession number: NM_000238.4), Kir1.1 (*Homo sapiens*, accession number: NM_000220.6), Kir2.1 (*Homo sapiens*, accession number: NM_000891.3), Kir4.1 (*Homo sapiens*, accession number: NM_002241.5), $Ca_V1.2$ (*Mus musculus*, accession number: NM_009781.4), $Ca_V2.2$ (*Rattus norvegicus*, accession number: NM_147141.3), $Ca_V3.1$ (*Homo sapiens*, accession number: NM_018896), ASIC1a (*Rattus norvegicus*, accession number: NM_024154), ASIC3 (*Rattus norvegicus*, accession number: NM_173135), H_V1 (*Homo sapiens*, accession number: NM_032369.4), and PAC (*Homo sapiens*, accession number: NM_018252.3) were subcloned in plasmids pCDNA3.1 or pCMV-blank. Otop1 mutants were made by site-directed mutation using KOD FX PCR kit (Toyobo Co., Ltd., Osaka, Japan) and FastDigest DpnI (Fermentas, Burlington, Canada). Briefly, the parental channel plasmid was amplified by a pair of oppositely directed mutation primers with a 15 bp overlap at their 5' ends, the PCR product was digested by DpnI to remove the template, and 10 μL digestion mix was used to transform 100 μL DH5α chemical competent cells. Plasmids from several transformants were extracted and sequenced to confirm that correct mutants were made.

Cell culture and transient transfection

HEK293T cells were from ATCC (ATCC Cat# CRL-3216, RRID:CVCL_0063). HEK293T-PAC$^{-/-}$ cells with the proton-activated chloride channel (PAC) gene knocked out were as described in our previous study[41]. HEK293T-PAC$^{-/-}$cells were used for expressing Otop and Otop mutant channels, and HEK293T cells for other ion channels. Cells were cultured in Dulbecco's Modified Eagle Medium (DMEM) supplemented with 10% FBS and 1% PS (all from Gibco; Thermo Fisher Scientific, Waltham, MA,USA), in standard cell culture conditions (37 °C, 5% CO_2, and saturated humidity). Transfection was conducted when the cell confluence reached 80%, using Lipofectamine 2000 following the manufacturer's instruction (Invitrogen; Thermo Fisher Scientific, Inc., Waltham, MA, USA). For wild-type Otop1, Otop2, Otop3, and Otop1 mutants, 2.5 μg channel plasmid was co-tranfected with 0.5 μg pEGFP-N1 plasmid expressing the green fluorescence protein (EGFP), for identifying the positively transfected cells; for other ion channels, the transfection amount was adjusted in a principle to record appropriate magnitude of currents. Cells were seeded onto PLL(poly-l-lysine)-coated coverslips 4–6 h post transfection, and patch-clamp experiments were performed after 16–24 h additional culture allowing for channel expression.

Electrophysiology

Whole-cell current recording was performed in a patch-clamp platform equipped with EPC-10 amplifier (HEKA Elektronik, Lambrecht, Germany) and MP-285 manipulator (SUTTER instrument, Novato, CA, USA). Data were acquired using PatchMaster software (HEKA Elektronik, Lambrecht, Germany). The recording pipette was made from glass capillary in a PC-10 puller (NARISHIGE, Tokyo, Japan), with resistance of 2–3 MΩ after filling with pipette solution. Whole-cell configuration was achieved by standard protocol. To minimize artificial capacitance effect, only the pipette tip was filled with pipette solution, and fast and slow capacitance was sequentially compensated using the computer-controlled circuit of the amplifier. Voltage error was minimized by keeping the serial resistance (Rs) after breaking in to be less than 10 MΩ, along with a 80% Rs compensation with a speed value of 10 μs. A 3 M KCl salt-bridge was also routinely used in our electrophysiological recordings.

For recording currents of Otop channels, the pipette solution contains (in mM): 120 Cs-aspartate, 15 CsCl, 2 Mg-ATP, 5 EGTA, 2.4 $CaCl_2$, and 10 HEPES (adjust pH to 7.3 with CsOH); the standard Tyrode solution contains (in mM):145 NaCl, 5 KCl, 2 $CaCl_2$, 1 $MgCl_2$, 20 D-Glucose, and 10 HEPES (adjust pH to 7.4 with NaOH); the bath solution of different pHs contains (in mM): 160 NMDG-Cl, 2 $CaCl_2$, and 10 Tris (pH 8.0–10.5), or 10 HEPES (pH 7.4), or 10 MES (pH 6.0–5.5), or 10 HomoPIPES (pH 5.0–4.0), pH adjusted with HCl. The adjustment of pH has a negligible effect on the Cl^- concentration in bath solution. For experiments in Fig. 4 analyzing the ion selectivity of Otop1, NMDG-Cl was substituted with NaCl, KCl, or CsCl.

For Na_V currents recording, the pipette solution contains (in mM): 140 CsF, 1 EGTA, 10 NaCl, and 10 HEPES (adjust pH to 7.4 with CsOH); and the corresponding bath solution contains (in mM): 140 NaCl, 5 KCl, 2 $CaCl_2$, 1 $MgCl_2$, 10 D-Glucose, and 10 HEPES (adjust pH to 7.4 with NaOH).

For K_V currents recording, the pipette solution contains (in mM): 140 KCl, 2.5 $MgCl_2$, 11 EGTA, and 10 HEPES (adjust pH to 7.4 with KOH); and the corresponding bath solution contains (in mM): 145 NaCl, 2.8 KCl, 2 $CaCl_2$, 1 $MgCl_2$, 10 D-Glucose, and 10 HEPES (adjust pH to 7.4 with NaOH).

For Ca_V currents recording, the pipette solution contains (in mM): 120 $CsMeSO_3$, 2 Mg-ATP, 11 EGTA, and 10 HEPES (adjust pH to 7.4 with CsOH); and the corresponding bath solution contains (in mM): 138 NaCl, 5.6 KCl, 2.6 $CaCl_2$, 20 TEA-Cl, 5 D-Glucose, and 5 HEPES (adjust pH to 7.4 with NaOH).

For Kir1.1, Kir2.1, and Kir4.1 currents recording, the pipette solution contains (in mM): 135 KCl, 2 $MgCl_2$, 10 HEPES, 1 EGTA, 4 Na_2-ATP (adjusting the pH to 7.3 with KOH); and the corresponding bath solutions contains (in mM): 135 NaCl, 5 KCl, 1.5 $CaCl_2$, 1 $MgCl_2$, 10 HEPES, 10 glucose (adjusting the pH to 7.4 with NaOH).

For ASIC1a and ASIC3 currents recording, the pipette solutions contains (in mM): 140 CsF, 11 EGTA, 1 $CaCl_2$, 2 TEA-Cl, 4 $MgCl_2$ and 10 HEPES (adjust pH to 7.3 with CsOH); and the corresponding bath solution contains (in mM): 140 NaCl, 5.4 KCl, 2 $CaCl_2$, 1 $MgCl_2$, 10 D-Glucose, and 20 HEPES (pH 7.4) or 20 MES (pH 5.5), adjust pH with NaOH.

For H_V1 currents recording, the pipette solutions contains (in mM): 120 CsCl and 100 MES (adjust pH to 5.5 with HCl); and the corresponding bath solution contains (in mM): 150 NaCl, 5 KCl, 1 $MgCl_2$, 2 $CaCl_2$, 10 D-Glucose, and 100 HEPES (adjust pH to 7.2 with NaOH).

For PAC currents recording, the pipette solutions contains (in mM): 135 CsCl, 1 $MgCl_2$, 2 $CaCl_2$, 10 HEPES, 5 EGTA and 4 Mg-ATP (adjust pH to 7.2 with CsOH); and the corresponding bath solution contains (in mM): 145 NaCl, 2 KCl, 2 $MgCl_2$, 1.5 $CaCl_2$, 10 D-Glucose, 10 HEPES (pH 7.3; adjust pH with NaOH), or 5 Na_3-citrate (pH 5.5; adjust pH with citric acid).

All chemicals were from Sigma-Aldrich (Sigma-Aldrich, Saint Louis, MO, USA). Acute perfusion of drugs or solutions was achieved using a pressurized ALA-VM4 perfusion system (ALA scientific instrument, NY, USA), with a optimized speed of fast replacement of the solution in the chamber (with a volume of approximately 200 uL) while not impairing the recording. Briefly, the solution in the perfusion chamber was removed by a

vacuum system connected tubing, and the substituting solutions were applied simultaneously by a perfusion pipette placed near the recording pipette. This operation was repeated twice to ensure complete replacement of the original solution in the chamber. The dose-response curves were fit using a Hill logistic equation: $Y = Y0 + (Ymax - Y0)/(1 + EC50/[X])$, where [X] represents the compound concentration, EC_{50} is the half-maximal effective concentration, and Y_{max} and Y_0 denote the the maximum and minimum repsonses, respectively.

Live cell pH fluorescence imaging

HEK293 cells used for fluorescence imaging were transfected by electroporation (Bio-Rad Gene Pulser Xcell system, Hercules, CA, USA). The electroporation protocol was a voltage step pulse (180 V, 25 ms) using 4 mm cuvettes. Transfected cells were seeded onto round coverslips and cultured with DMEM. Imaging experiments were carried out 24 h after transfection. Time-lapse fluorescence imaging experiments were performed with a ZEISS observer Z1 imaging system controlled by SlideBook v.6.0.23 software (Intelligent Imaging Innovations, Inc.). Cells seeded on coverlips were imaged in a physiological salt solution (in mM: 140 KCl, 10 NaCl, 1 $MgCl_2$, and 20 HEPES/pH 7.4) to mimic intracellular ironic environment, and stimulus solutions of different pHs were made by replacing HEPES with Tris (pH8.5), MES (pH6.0), or Homo-PIPES (pH5.0). Filters: pHmScarlet (RFP channel), 500 ± 12 nm_{ex}/542 ± 13 nm_{em}; mTurquise2 (CFP channel), 438 ± 12 nm_{ex}/470 ± 12 nm_{em}. The fluorescence was collected every two seconds, and the mean fluorescence ratio (R=FpHmScarlet/FmTurquise2) of the corresponding regions was calculated and exported for analysis using Matlab 2023b (The MathWorks, Natick, MA, USA).

Data analysis

Data are presented as MEAN ± SEM. *n* represents the number of independent experimental cells, each of which represents a biological replicate. Data were analyzed using Igor Pro 6.10 A (WaveMetrics, Inc., Lake Oswego, OR, USA), Sigmaplot 10.0 (Systat Software, Inc., San Jose, CA, USA), and GraphPad Prism 9.0 (GraphPad Software, Inc., La Jolla, CA, USA).

Statistics and reproducibility

Statistical analyses were performed using two-tailed paired or unpaired t-tests, or one-way ANOVA followed by post-hoc Dunnett's or Tukey's tests, as appropriate. A *p*-value of less than 0.05 was considered statistically significant. Significance levels are indicated as follows: $*p < 0.05$, $**p < 0.01$, $***p < 0.001$, and $****p < 0.0001$. All repetitions are performed independently, the legend in the figure shows the specific repeated values (*n* values). In Fig. 1C, all data points are obtained from 5 separate experimental cells. In Fig. 1J, the sample sizes for each concentration are as follows: 1 μM, $n = 6$; 5 μM, $n = 6$; 10 μM, $n = 7$; 50 μM, $n = 4$, 100 μM, $n = 5$. The source data underlying Figs. 1C, E, G, H, J, 2A–F, 3A, B, 4A, B, D, F, G, 5A, D, F, H, J, and Supplementary Figs. 7B and 8 can be found in supplementary Data 1.

Reporting summary

Further information on research design is available in the Nature Portfolio Reporting Summary linked to this article.

Data availability

The data supporting this study are available from the corresponding authors on reasonable request. All data are included in the article and supplementary information files, The source data underlying Figs. 1C, E, G, H, J, 2A–F, 3A, B, 4A, B, D, F, G, 5A, D, F, H, J, and Supplementary Figs. 7B and 8 can be found in supplementary data 1.

Received: 16 September 2024; Accepted: 18 February 2025;
Published online: 26 February 2025

References

1. Hille, B. J. S. A. Ion Channels of Excitable Membranes. (2001).
2. Zeng, W. Z. & Xu, T. L. Proton production, regulation and pathophysiological roles in the mammalian brain. *Neurosci. Bull.* **28**, 1–13 (2012).
3. Yang, J. et al. PAC, an evolutionarily conserved membrane protein, is a proton-activated chloride channel. *Sci. (N.Y., N.Y.)* **364**, 395–399 (2019).
4. Waldmann, R., Champigny, G., Bassilana, F., Heurteaux, C. & Lazdunski, M. A proton-gated cation channel involved in acid-sensing. *Nature* **386**, 173–177 (1997).
5. Aneiros, E. et al. The biophysical and molecular basis of TRPV1 proton gating. *EMBO J.* **30**, 994–1002 (2011).
6. Carmona, E. M. et al. The voltage sensor is responsible for ΔpH dependence in H(v)1 channels. *Proc. Natl. Acad. Sci. USA.* **118**, https://doi.org/10.1073/pnas.2025556118 (2021).
7. Cherny, V. V., Morgan, D., Thomas, S., Smith, S. M. E. & DeCoursey, T. E. Histidine(168) is crucial for ΔpH-dependent gating of the human voltage-gated proton channel, hH(V)1. *J. Gen. Physiol.* **150**, 851–862 (2018).
8. Peters, C. H., Ghovanloo, M. R., Gershome, C. & Ruben, P. C. pH Modulation of Voltage-Gated Sodium Channels. *Handb. Exp. Pharmacol.* **246**, 147–160 (2018).
9. Jordt, S. E., Tominaga, M. & Julius, D. Acid potentiation of the capsaicin receptor determined by a key extracellular site. *Proc. Natl. Acad. Sci. USA* **97**, 8134–8139 (2000).
10. Sasaki, M., Takagi, M. & Okamura, Y. A voltage sensor-domain protein is a voltage-gated proton channel. *Science. (N.Y., N.Y.)* **312**, 589–592 (2006).
11. Breslin, P. A. An evolutionary perspective on food and human taste. *Curr. Biol.: CB* **23**, R409–418 (2013).
12. Nelson, G. et al. Mammalian sweet taste receptors. *Cell* **106**, 381–390 (2001).
13. Li, X. et al. Human receptors for sweet and umami taste. *Proc. Natl. Acad. Sci. USA* **99**, 4692–4696 (2002).
14. Taruno, A. & Gordon, M. D. Molecular and Cellular Mechanisms of Salt Taste. *Annu. Rev. Physiol.* **85**, 25–45 (2023).
15. Chandrashekar, J. et al. T2Rs function as bitter taste receptors. *Cell* **100**, 703–711 (2000).
16. Zhang, J. et al. Sour Sensing from the Tongue to the Brain. *Cell* **179**, 392–402.e315 (2019).
17. Teng, B. et al. Cellular and Neural Responses to Sour Stimuli Require the Proton Channel Otop1. *Curr. Biol. : CB* **29**, 3647–3656.e3645 (2019).
18. Hughes, I. et al. Otopetrin 1 is required for otolith formation in the zebrafish Danio rerio. *Developmental Biol.* **276**, 391–402 (2004).
19. Chang, R. B., Waters, H. & Liman, E. R. A proton current drives action potentials in genetically identified sour taste cells. *Proc. Natl. Acad. Sci. USA* **107**, 22320–22325 (2010).
20. Bushman, J. D., Ye, W. & Liman, E. R. A proton current associated with sour taste: distribution and functional properties. *FASEB J. : Off. Publ. Federation Am. Soc. Exp. Biol.* **29**, 3014–3026 (2015).
21. Tu, Y. H. et al. An evolutionarily conserved gene family encodes proton-selective ion channels. *Science* **359**, 1047–1050 (2018).
22. Teng, B. et al. Structural motifs for subtype-specific pH-sensitive gating of vertebrate otopetrin proton channels. *eLife* **11**, https://doi.org/10.7554/eLife.77946 (2022).
23. Chen, Q., Zeng, W., She, J., Bai, X. C. & Jiang, Y. Structural and functional characterization of an otopetrin family proton channel. *eLife* **8**, https://doi.org/10.7554/eLife.46710 (2019).
24. Saotome, K. et al. Structures of the otopetrin proton channels Otop1 and Otop3. *Nat. Struct. Mol. Biol.* **26**, 518–525 (2019).
25. Huang, J., Pan, X. & Yan, N. Structural biology and molecular pharmacology of voltage-gated ion channels. *Nat. Rev. Mol. cell Biol.* **25**, 904–925 (2024).
26. Cao, E. Structural mechanisms of transient receptor potential ion channels. *J. General Physiol.* **152**, https://doi.org/10.1085/jgp.201811998 (2020).

27. Li, B. et al. The roles of two extracellular loops in proton sensing and permeation in human Otop1 proton channel. *Commun. Biol.* **5**, 1110 (2022).
28. Tian, L. et al. Vertebrate OTOP1 is also an alkali-activated channel. *Nat. Commun.* **14**, 26 (2023).
29. Liang, Z., Wilson, C. E., Teng, B., Kinnamon, S. C. & Liman, E. R. The proton channel OTOP1 is a sensor for the taste of ammonium chloride. *Nat. Commun.* **14**, 6194 (2023).
30. Teng, B. et al. Zinc activation of OTOP proton channels identifies structural elements of the gating apparatus. *eLife* **12**, https://doi.org/10.7554/eLife.85317 (2023).
31. Islam, M. M., Sasaki, O., Yano-Nashimoto, S., Okamatsu-Ogura, Y. & Yamaguchi, S. Cibacron blue 3G-A is a novel inhibitor of Otopetrin 1 (OTOP1), a proton channel. *Biochemical biophysical Res. Commun.* **665**, 64–70 (2023).
32. Roberts, C. D., Dvoryanchikov, G., Roper, S. D. & Chaudhari, N. Interaction between the second messengers cAMP and Ca2+ in mouse presynaptic taste cells. *J. Physiol.* **587**, 1657–1668 (2009).
33. Gao, N. et al. Voltage-gated sodium channels in taste bud cells. *BMC Neurosci.* **10**, 20 (2009).
34. Ohtubo, Y. Slow recovery from the inactivation of voltage-gated sodium channel Nav1.3 in mouse taste receptor cells. *Pflug. Arch. : Eur. J. Physiol.* **473**, 953–968 (2021).
35. Colquhoun, D. Binding, gating, affinity and efficacy: the interpretation of structure-activity relationships for agonists and of the effects of mutating receptors. *Br. J. Pharm.* **125**, 924–947 (1998).
36. Noh, S. et al. The direct modulatory activity of zinc toward ion channels. *Integr. Med. Res.* **4**, 142–146 (2015).
37. Peralta, F. A. & Huidobro-Toro, J. P. Zinc as Allosteric Ion Channel Modulator: Ionotropic Receptors as Metalloproteins. *Int. J. Mol. Sci.* **17**, https://doi.org/10.3390/ijms17071059 (2016).
38. Hu, J. et al. Gating elements for carvacrol activation of the OTOP1 proton channel. *Commun. Biol.* **7**, 1106 (2024).
39. Yelshanskaya, M. V., Patel, D. S., Kottke, C. M., Kurnikova, M. G. & Sobolevsky, A. I. Opening of glutamate receptor channel to subconductance levels. *Nature* **605**, 172–178 (2022).
40. Pan, X., Wang, H., Li, C., Zhang, J. Z. H. & Ji, C. MolGpka: A Web Server for Small Molecule pK(a) Prediction Using a Graph-Convolutional Neural Network. *J. Chem. Inf. Model* **61**, 3159–3165 (2021).
41. Zhao, P. et al. A new polymodal gating model of the proton-activated chloride channel. *PLoS Biol.* **21**, e3002309 (2023).
42. Gan, N., Zeng, W., Han, Y., Chen, Q. & Jiang, Y. Structural mechanism of proton conduction in otopetrin proton channel. *Nat. Commun.* **15**, 7250 (2024).

Acknowledgements

This work was supported by the National Natural Science Foundation of China (Grant Nos. 31600669, 32071262, 32171271, and 91954205), the Science and Technology Innovation Program of Hunan Province (2020RC4023), the Natural Science Foundation of Hunan Province (Grant No. 2018JJ3339), and the Research Foundation of the Education Department of Hunan Province (Grant Nos. 18B015 and 22A0076).

Author contributions

C.T. developed the concept and designed the experiments. C.T. and Z.L. jointly supervised the study. C.T. and Y.W. analyzed the data, and drafted and revised the manuscript. C.T., X.K., J.S., H.Z., Y.Y., X.L., Y.C., G.L., and H.X. conducted the experiments. C.T., Z.L., and Y.W. secured funding. All authors contributed to discussing the results and reviewing the manuscript.

Competing interests

The authors declare no competing interests.

Additional information

Supplementary information The online version contains supplementary material available at https://doi.org/10.1038/s42003-025-07775-9.

Correspondence and requests for materials should be addressed to Zhonghua Liu or Cheng Tang.

Peer review information *Communications Biology* thanks Tharaka Darshana Wijerathne and the other, anonymous, reviewers for their contribution to the peer review of this work. Primary Handling Editors: Yun Luo and Laura Rodríguez Pérez. [A peer review file is available].